06/02/2026

Crowder architecture matters: Distinct effects of linear and branched macromolecular crowders on dynamics and function of *Escherichia coli* prolyl-tRNA synthetase

Gaona Her, Breanna Hayden, Brianna Finke, Elijah Weitzel, Christine Le, Anne S. Moise, Sudeep Bhattacharyya*, and Sanchita Hati*

Department of Chemistry and Biochemistry, University of Wisconsin-Eau Claire, Eau Claire, WI, 54701, USA

*E-mail: bhattas@uwec.edu; hatis@uwec.edu.

Table of contents

Keywords

Conformational dynamics; dextran 40; ficoll 70; intrinsic tryptophan fluorescence; molecular crowding; molecular dynamics simulations; prolyl-tRNA synthetase; saturation transfer difference-nuclear magnetic resonance spectroscopy

Abbreviations

Adenosine Triphosphate, ATP; Barycentric Mean Wavelength, l_{BCM}; Catalytic Domain, CD; *Escherichia coli* Prolyl-tRNA Synthetase, Ec ProRS; Editing Domain, ED; Molecular Dynamics, MD; Polyethylene Glycol, PEG; Saturation Transfer Difference-Nuclear Magnetic Resonance, STD-NMR; Stern-Volmer Plots, S-V Plots; Subunit A, SUB A; Subunit B, SUB B; Wild-type, WT.

Experimental Procedure

All reagents were obtained from either Sigma-Aldrich or ThermoFisher Scientific; ficoll 70 was purchased from Cytiva. Ec ProRS was purified through a multi-step process, and the concentration was determined as described earlier.[1]

Intrinsic fluorescence spectroscopy

Intrinsic fluorescence measurements were carried out for Ec ProRS (1 μM) in 100 mM NaCl and 30 mM phosphate buffer (pH 7.4) with varying crowder concentrations (100–300 mg/mL), following published procedures.[1] Samples were excited at 295 nm, and emission spectra (300–400 nm) were recorded in a 1-cm quartz cuvette using an Agilent Cary Eclipse spectrophotometer. Samples and blanks were incubated at 20 °C or 35 °C for 30 min, and measurements were performed in 2–3 replicates. Spectra were blank-corrected by subtracting corresponding buffer measurements. Fluorescence intensity and barycentric mean values were analyzed as discussed in the recently published work of Liebau *et al.*[1] Stern–Volmer plots were generated to examine crowder-induced quenching mechanisms. PEG 20 was excluded due to stabilizer interference with Ec ProRS fluorescence.[2]

Thermal protein unfolding or melting experiments

Thermal unfolding of Ec ProRS was measured in the presence of various crowders (Fig. S1) to assess their effects on protein stability. Fluorescence spectra were collected at 3 °C intervals from 25 °C to 76 °C, and melting temperatures were determined by plotting temperature versus barycentric mean, as described previously.[1] Data were fitted to a Boltzmann S-curve using

OriginPro 2021 [Origin Lab Corporation, Northampton, MA, USA]. All experiments were performed in duplicate.

Saturation Transfer Difference-Nuclear Magnetic Resonance (STD-NMR) spectroscopy

STD-NMR is a powerful ligand-based NMR technique for the study of protein-ligand interactions and determining K_D values.[3–5] This technique was used to assess ATP binding to Ec ProRS, following established principles in which selective saturation of protein resonances is transferred to ligand protons upon binding, yielding an STD spectrum that highlights only receptor-interacting ligand.[4] Briefly, in an STD-NMR experiment, the resonances of the receptor molecule (i.e., the target protein) are selectively saturated, and this saturation rapidly spreads throughout the protein via spin diffusion.[6] When a ligand binds to the protein, saturation is transferred primarily to the ligand protons that are in closest proximity to the protein.[7,8] Upon dissociation, the saturated ligand molecules return to the bulk solution, resulting in a reduction of their NMR signal intensity. The difference between the reference spectrum (recorded without saturation) and the saturated spectrum yields the STD spectrum, which displays signals exclusively from ligand molecules that have interacted with the receptor protein.[5,6]

For STD-NMR experiments, WT Ec ProRS was overexpressed and purified using Talon cobalt affinity resin, exchanged into buffer containing 50 mM HEPES, 300 mM NaCl, and 2 mM DTT (pH 7.5), concentrated, and stored at –20 °C with glycerol and DTT; all solutions were made in D_2O. Samples contained 0.1 mM Ec ProRS, 100 mg/mL crowder, and 1–10 mM ATP in the same buffer system used for fluorescence studies. STD-NMR experiments were recorded at room temperature on a Bruker Avance II 400 MHz spectrometer using 1024 scans, a 2 s saturation time, 2.1 s delay, and 0.3 Hz line broadening. On-resonance saturation was applied at –2 ppm and off-resonance at +40 ppm. STD spectra ($I_{off} - I_{on}$) were obtained by subtracting saturated from

reference spectra, and fractional STD effects were calculated as $(I_{off} - I_{on}) / I_{off}$. ATP binding was quantified by integrating the 8.175 ppm ATP peak (Fig. S2), with appropriate blanks confirming absence of direct ligand irradiation. The STD-amplification factor (A_{STD}) was calculated using

$$A_{STD} = \left(\frac{I_{off} - I_{on}}{I_{off}}\right)\left(\frac{[ATP]}{[E]}\right) \#(1)$$

The dependence of A_{STD} on ATP concentration was fit to

$$A_{STD} = \frac{\alpha_{STD} * [ATP]}{K_D + [ATP]} \#(2)$$

for determining dissociation constants (K_D). In Eq (2), α_{STD} represents the maximum amplification factor, [ATP] is the substrate concentration, and K_D is the dissociation constant.[5] Measurements were conducted in the presence and absence of PEG 20, dextran 40, and ficoll 70 to evaluate crowding effects on ATP binding by developing the binding curve (Fig. S3).[4,9]

Viscosity measurement

Aqueous solutions of PEG 20, dextran 40, and ficoll 70 (100 mg/mL) were prepared for viscosity measurements, which were conducted at 20 °C using a TA Instrument DHR-2 Rheometer system with a 2° upper cone geometry. All measurements were performed in triplicate using 0.7 mL aqueous solutions of crowders.

Molecular dynamics simulations

All computations were caried out using in-house GPU-CPU BOSE cluster.[10] Molecular visualization and editing were carried out using Visual Molecular Dynamics (VMD).[11] Molecular dynamics (MD) simulations were carried out with NAMD[12,13] using procedures as described earlier.[1] The molecular models of dextran 40 and ficoll 70 molecules were generated following

procedures outlined in the study of Ostrowska *et al*. [14] PEG crowder molecules as well as all solvated crowder-enzyme models were carried out using procedures described earlier.[1] All simulations are carried out using CHARMM36[15–17] all-atom forcefield, while maintaining all core simulation technics as elaborated in the study of PEG crowders by Liebau *et al.*[1]

Protein and polymer crowders were manually added to the dimeric protein structure to generate three assemblies: ProRS with 18 PEG eight strands, ProRS with eight PEG 20 strands, ProRS with four dextran 40 strands, and ProRS with two ficoll 70 strands. The number of crowders strands included in MD simulations was adjusted to match the experimental conditions and to maintain an approximate crowder concentration of ~100 mg/mL. The solvated crowder-protein assemblies are depicted in Fig. S4. The generated assemblies were simulated for 100 ns using atomistic MD simulations and animations comprising five frames that illustrate the evolution of the ProRS-crowder assemblies are given in Fig. S7. The ATP-containing crowder assemblies were generated with eight PEG 20 strands, four dextran 40 strands, and two ficoll 70 strands. In each of these systems, one ATP molecule was manually placed within van der Waals contact of the surrounding crowder atoms. All structures were solvated in a water box so that all water molecules within 2.4 Å distance from the protein atoms were eliminated. The solvated crowder-ATP assemblies are depicted in Fig. S8, respectively.

Table S1. The percent decrease in tryptophan (Trp) fluorescence intensity of 1 μM Escherichia coli ProRS in the presence of 200 mg/mL of macromolecular crowders, compared to the dilute condition, was measured. Protein samples were excited at 295 nm, and fluorescence emissions were recorded between 300–400 nm. The shift in barycentric mean wavelength ($\Delta\lambda_{bcm}$) was determined as described earlier (Ref. 36). All data represent the average of three independent trials, with standard deviations within 5%. As discussed in Laatsch et al. (Ref. 47) PEG 20k was excluded due to stabilizer interference with Ec ProRS fluorescence.

Crowder	**% Decrease**	**$\Delta\lambda_{bcm}$ (n.m)**
PEG 8	19.8	0.4
dextran 40	49.7	0.9
ficoll 70	64.6	1.4

Table S2. The melting temperature of Ec ProRS in the presence of 200 mg/mL crowders (crowded environments) compared to that in buffer (dilute condition).[a]

System	T_m
ProRS without crowders	48.9 ± 0.5 °C
ProRS + PEG 8[b]	53.6 ± 0.4 °C
ProRS + dextran 40	51.9 ± 0.8 °C
ProRS + ficoll 70	53.8 ± 0.7 °C

[a]The concentration of Ec ProRS was 1 μM. The fluorescence emissions were collected at 3 °C intervals from 25 to 76 °C with an excitation wavelength of 295 nm. The melting temperatures were determined by plotting the barycentric mean wavelength against the temperature (as discussed in Liebau *et al*. (Ref. 36). Experiments were performed in triplicate, with the standard deviation indicated.

[b]The data obtained from Ref. 36

Table S3. The viscosity (in Pa.s) of an aqueous solution containing 100 mg/mL of crowders; water viscosity: 1.00×10^{-3} Pa.s.

Trial	PEG 20	Dextran 40	ficoll 70
1	0.00890	0.00476	0.00297
2	0.0161	0.00527	0.00365
3	0.0181	0.00540	0.00327
Average	0.0143	0.00514	0.00330
S.D.	0.0048	0.00034	0.00034

Table S4. Details of the protein-crowder assembly generated to study effects of polymer crowders.

System built	Water atoms	Crowder atoms	Protein atoms	Dimensions of the orthorhombic box ($Å^3$)
dilute ProRS	263907	0	17692	155×150×124
ProRS + PEG 8	649578	23112	17692	208×180×200
ProRS + PEG 20	880296	25392	17692	199×236×194
ProRS + dextran 40	759018	20172	17692	186×226×200
ProRS + ficoll 70	452916	18662	17692	230×144×152
ATP + PEG 20	564069	25392	0	204×168×188
ATP+ ficoll 70	148740	18662	0	106×104×162
ATP + dextran 40	173748	20172	0	114×122×148

Table S5. Decomposition of interaction energy between crowder and protein and crowder and water, calculated for Ec ProRS in the presence of various crowders using conformations stored in trajectories two independent MD simulations. Uncertainties were calculated from fluctuations observed across two independent data sets.

Simulated systems / Interacting subsystems	Interaction energies (10^3 kcal/mol)		
	electrostatic	vdW	total
ProRS···PEG 8	–0.5 ± 0.1	–1.7 ± 0.4	–2.2 ± 0.6
ProRS···PEG 20	–0.101 ± 0.006	–0.45 ± 0.04	–0.55 ± 0.04
ProRS···dextran 40	–0.51 ± 0.03	–0.19 ± 0.04	–0.70 ± 0.07
ProRS···ficoll 70	–0.24 ± 0.03	–0.126 ± 0.003	–0.37 ± 0.03
water···PEG 8	–3.3 ± 0.2	–3.6 ± 0.3	–6.9 ± 0.4
water ···PEG 20	–3.18 ± 0.06	–3.7 ± 0.2	–7.0 ± 0.2
water···dextran 40	–27.2 ± 0.2	–3.837 ± 0.003	–31.1 ± 0.2
water ···ficoll 70	–26.4 ± 0.2	–4.06 ± 0.04	–30.4 ± 0.2

Table S6. The distribution of "open" and "closed" conformations for the dimeric Ec ProRS enzyme under various polymer crowders observed in 100 ns MD simulations. The "open" and "closed" conformations were determined from the stored trajectory of conformations using the distance of separation between C_α atoms of residues Q88 (on catalytic domain) and P318 (on editing domain). Based on the previously published study, the "open" conformation was defined as the Q88(C_α)-P318(C_α) distance was greater than 15 Å (Ref. 36).

Crowder	**ProRS subunit A**		**ProRS subunit B**	
	Open (%)	**Closed (%)**	**Open (%)**	**Closed (%)**
dilute [a]	79	21	73	27
PEG 20[a]	1	99	92	8
Dextran 40	0	100	95	5
Ficoll 70	48	52	12	88

[a] Taken from previously published literature (Ref. 36)

Figure S1. The three-dimensional (top panel) and chemical structure (bottom panel) of polymer crowders used: a) PEG 20, b) dextran 40, and c) ficoll 70. The carbon and oxygen atoms are colored as green and red, respectively, in the three-dimensional structure.

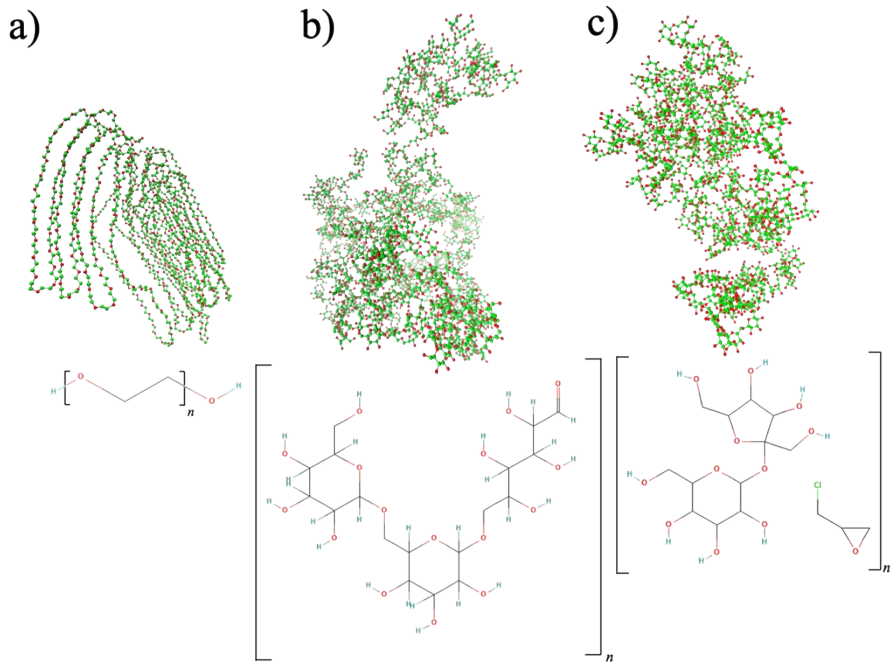

Figure S2. Saturation transfer difference (STD) NMR spectra of ATP in the presence of the protein. The reference (STD-off) spectrum (blue) displays the full set of ATP proton resonances in solution. The STD spectrum (red) shows signals corresponding only to ATP protons in close contact with the protein, demonstrating ATP binding. For the present study, ATP binding was quantified by integrating the ATP peak at 8.175 ppm (indicated by label 2 and the black arrow).

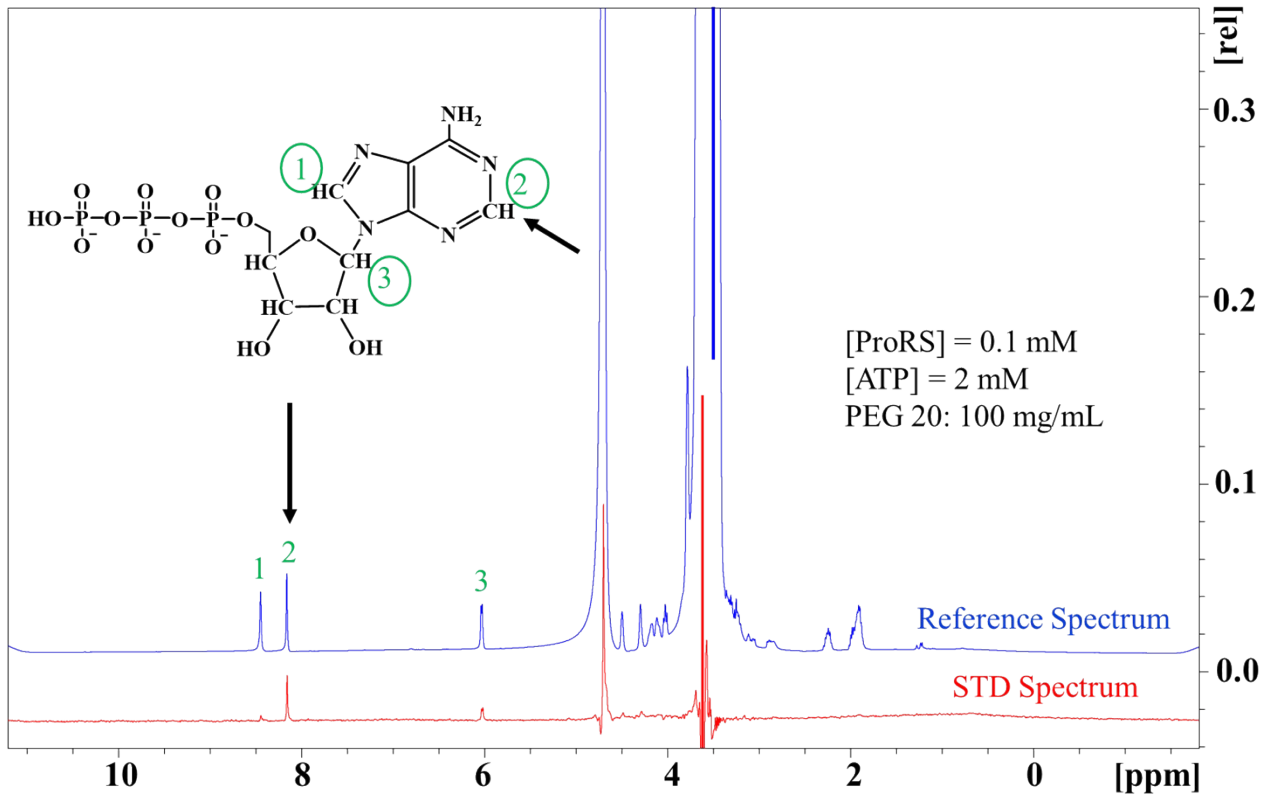

Figure S3. The binding curve was generated using STD-NMR data. The STD-NMR experiments were conducted using 0.1 mM Ec ProRS, in 30 mM phosphate buffer, pH 7.4, containing 100 mM NaCl, 100 mg/mL synthetic crowder, and varied ATP concentrations (1-10 mM). Amplification of STD effects with increasing ATP concentration was used to determine the binding affinities. In particular, the dissociation constants (K_D) for the ProRS–ATP complex in the presence of various molecular crowders were obtained from single-ligand titration STD-NMR experiments performed at six ATP concentrations ranging from 1 to 10 mM, using a constant saturation time of 2.0 s. By monitoring the increase in the STD amplification factor (A_{STD}) during titration, the K_D values were calculated according to Eq. 2.[9]

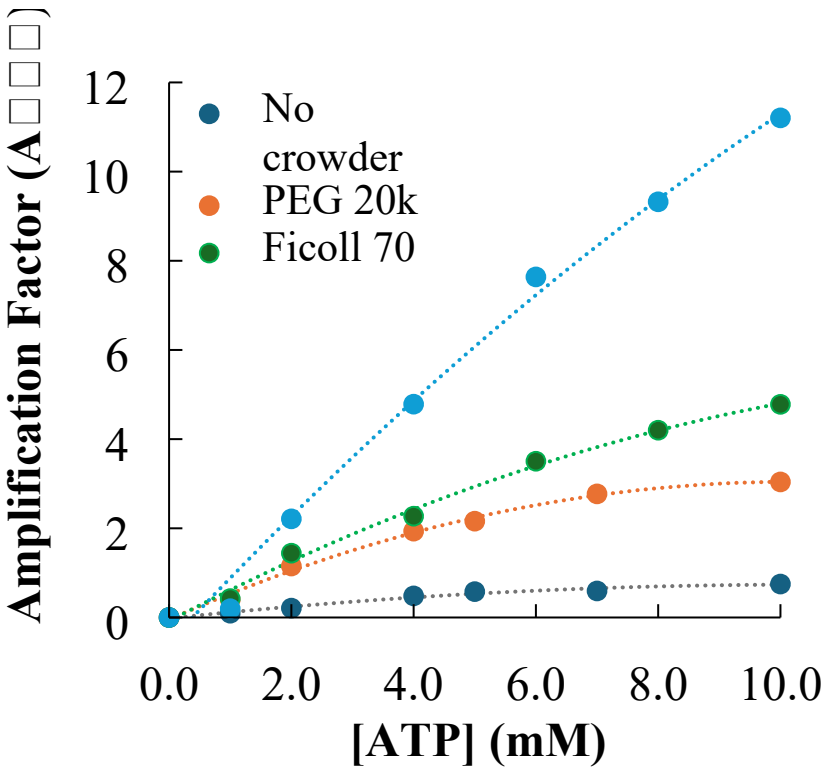

Figure S4. Model-systems for MD simulations were built with ProRS dimer and polymeric crowder molecules: (a) PEG 8, (b) PEG 20, (c) dextran 40, and (d) ficoll 70. The ProRS dimer is shown in cartoon representation, with distinct colors highlighting its three domains: ED (pink), CD (cyan), anticodon binding domain (green).

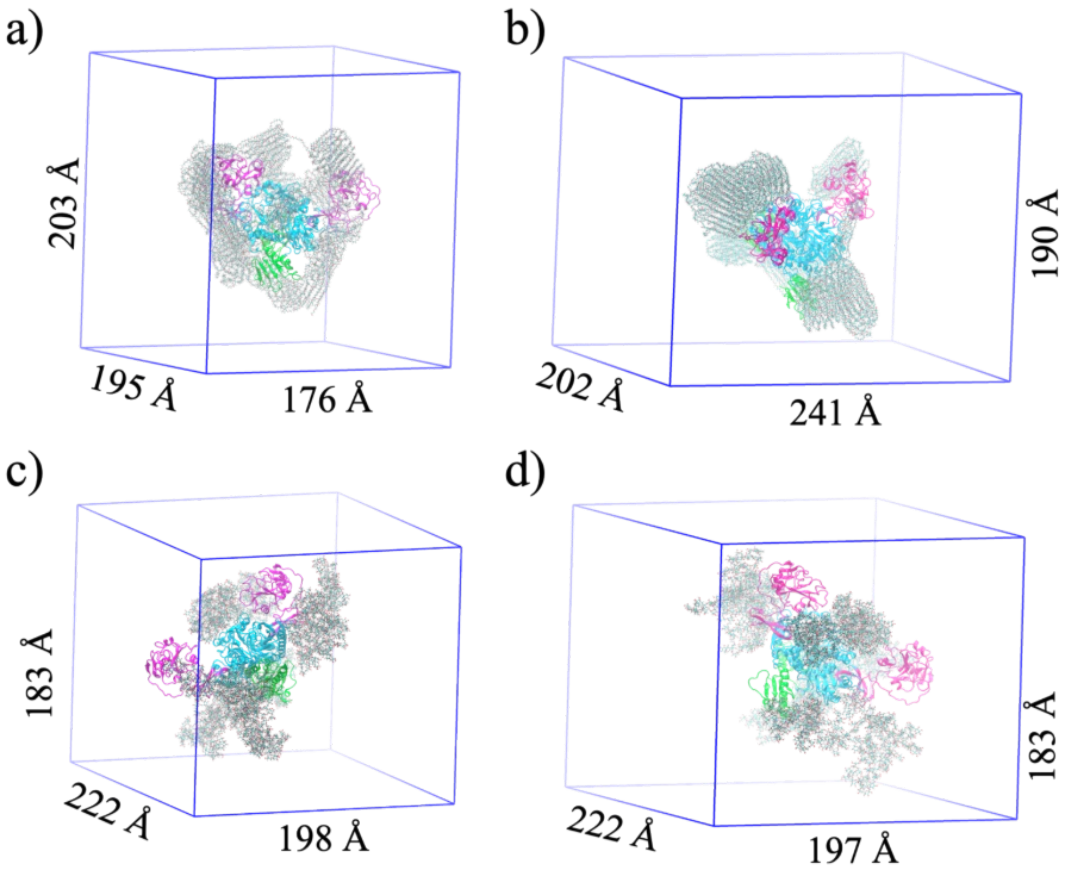

Figure S5. Decomposition of pair-wise interaction energy between a) protein-crowder and b) crowder-solvent systems. These energies are averaged from data of two independent simulations. Details are provided in Table S5.

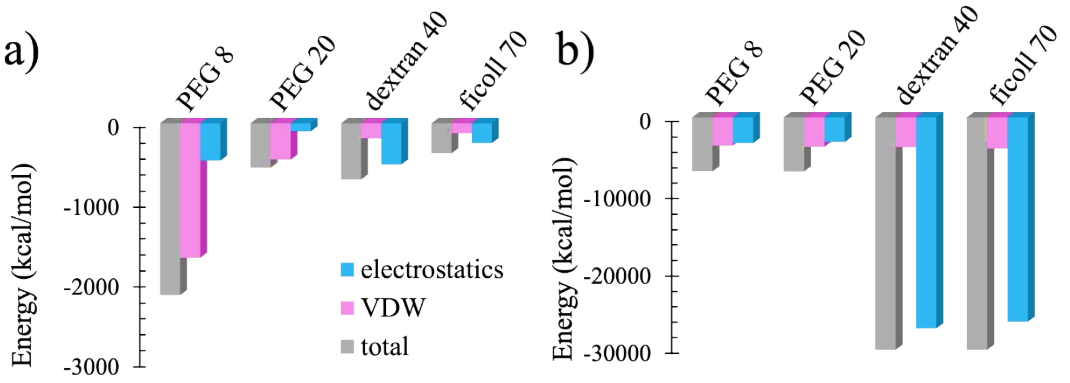

Figure S6. The number of protein-crowders H-bonding interactions, detected in the simulated system with synthetic crowders: a) dextran 40, b) ficoll 70, c) PEG 8, and d) PEG 20. The cut-offs for all interactions were kept at a maximum of 3 Å. The average values of H-bonds were calculated over 5 ns period of simulation are shown with a red dotted line.

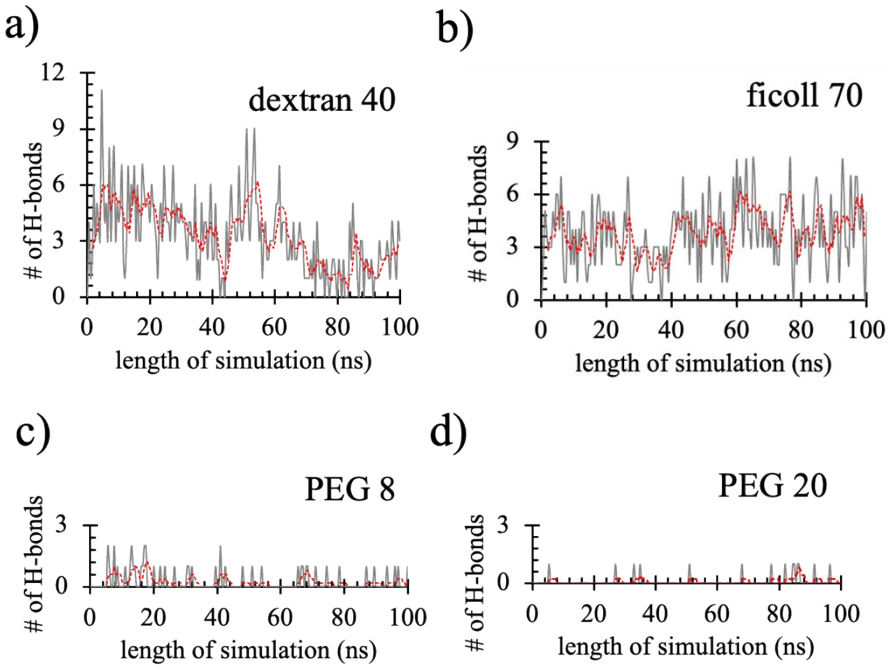

Figure S7. Short animations of 100 ns MD simulations of ProRS in the presence of polymer crowders: a) dextran 40, b) ficoll 70, c) PEG 8, d) PEG 20. Each animation contains five frames collected in 20 ns intervals. The ProRS dimer is shown in cartoon representation, with distinct colors highlighting its three domains: ED (pink), CD (cyan), and anticodon binding domain (orange).

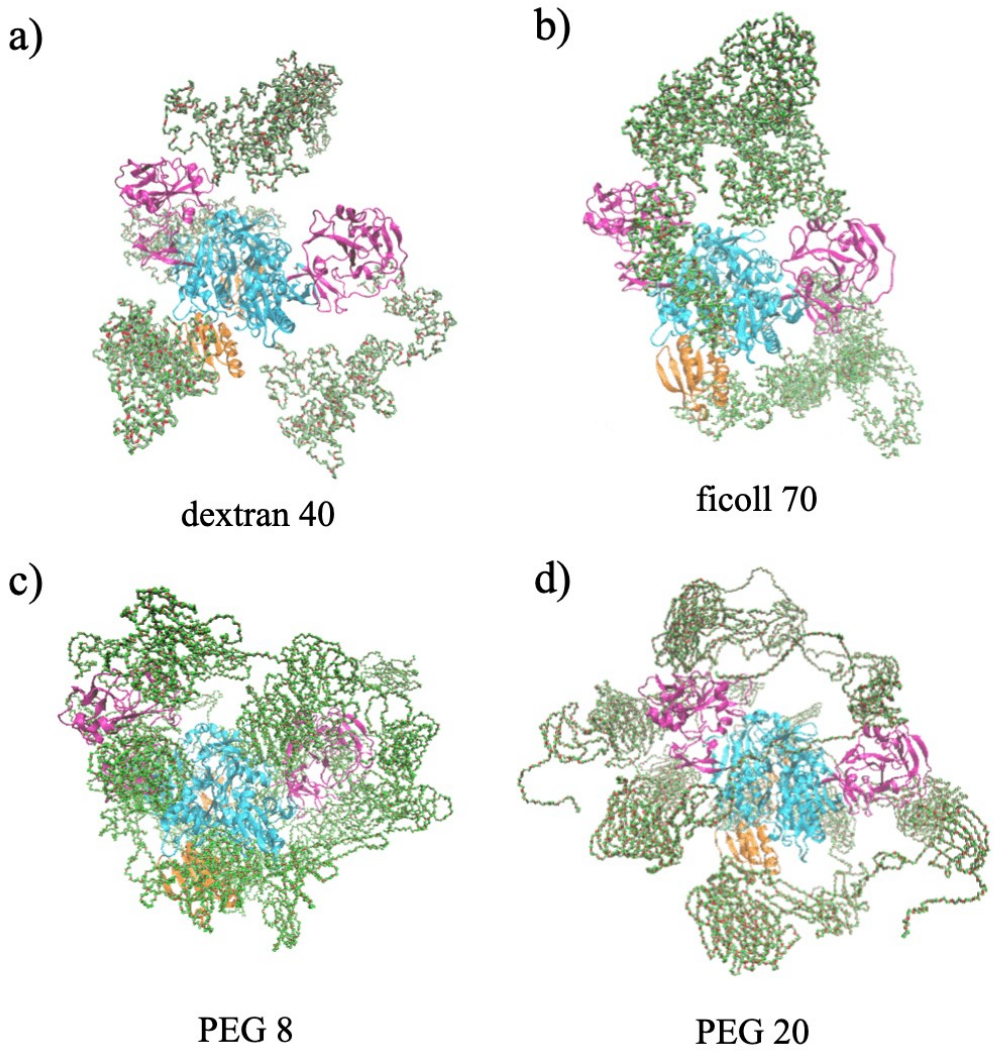

Figure S8. ATP-bound polymer crowder systems for MD simulations: a) ATP + eight PEG 20, b) ATP + four dextran 40, and c) ATP + two ficoll 70.

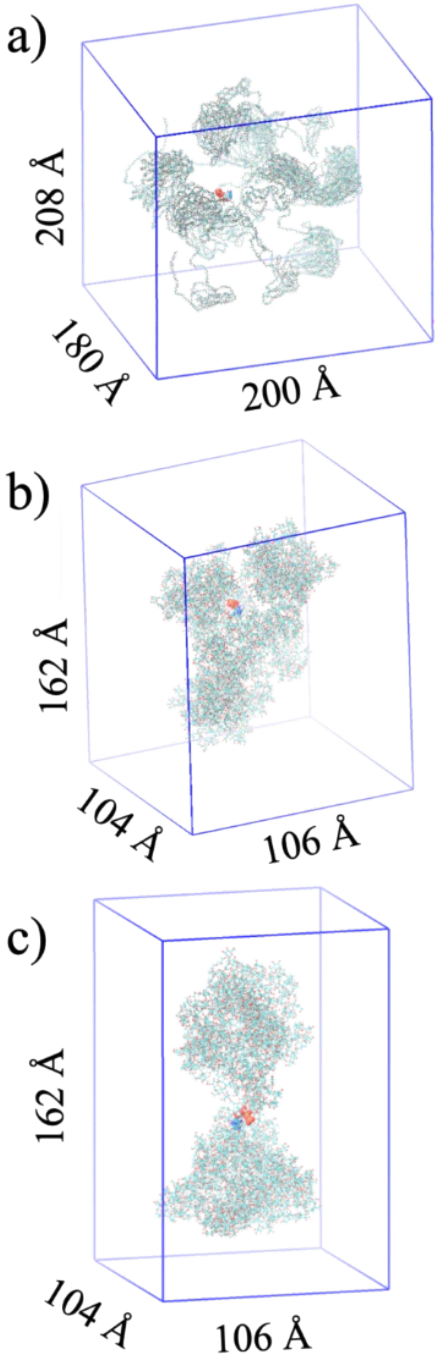

References

1 J. Liebau, B. F. Laatsch, J. Rusnak, K. Gunderson, B. Finke, K. Bargender, A. Narkiewicz-Jodko, K. Weeks, M. T. Williams, I. Shulgina, K. Musier-Forsyth, S. Bhattacharyya and S. Hati, Polyethylene Glycol Impacts Conformation and Dynamics of *Escherichia coli* Prolyl-tRNA Synthetase Via Crowding and Confinement Effects, *Biochemistry*, DOI:10.1021/acs.biochem.3c00719.

2 B. F. Laatsch, M. Brandt, B. Finke, C. J. Fossum, M. J. Wackett, H. R. Lowater, A. Narkiewicz-Jodko, C. N. Le, T. Yang, E. M. Glogowski, S. C. Bailey-Hartsel, S. Bhattacharyya and S. Hati, Polyethylene Glycol 20k. Does It Fluoresce?, *ACS Omega*, 2023, **8**, 14208–14218.

3 S. Maity, R. K. Gundampati and T. K. S. Kumar, NMR methods to characterize protein-ligand interactions, *Nat. Prod. Commun.*, 2019, **14**, 1–7.

4 J. L. Hall, A. Sohail, E. J. Cabrita, C. Macdonald, T. Stockner, H. H. Sitte, J. Angulo and F. MacMillan, Saturation transfer difference NMR on the integral trimeric membrane transport protein GltPh determines cooperative substrate binding, *Sci. Rep.*, 2020, **10**, 16483.

5 A. Viegas, J. Manso, F. L. Nobrega and E. J. Cabrita, Saturation-transfer difference (STD) NMR: A simple and fast method for ligand screening and characterization of protein binding, *J. Chem. Educ.*, 2011, **88**, 990–994.

6 J. L. Hall, A. Sohail, E. J. Cabrita, C. Macdonald, T. Stockner, H. H. Sitte, J. Angulo and F. MacMillan, Saturation transfer difference NMR on the integral trimeric membrane transport protein GltPh determines cooperative substrate binding, *Sci. Rep.*, 2020, **10**, 16483.

7 M. Mayer and B. Meyer, Characterization of ligand binding by saturation transfer difference NMR spectroscopy, *Angew. Chem. Int. Ed.*, 1999, **38**, 1784–1788.

8 M. Mayer and B. Meyer, Group epitope mapping by saturation transfer difference NMR to identify segments of a ligand in direct contact with a protein receptor, *J. Am. Chem. Soc.*, 2001, **123**, 6108–6117.

9 A. Kotar, T. Tomašič, M. Lenarčič Živković, G. Jug, J. Plavec and M. Anderluh, STD NMR and molecular modelling insights into interaction of novel mannose-based ligands with DC-SIGN, *Org. Biomol. Chem.*, 2016, **14**, 862–875.

10 J. Hebert, R. Hratisch, R. Gomes, W. Kunkel, D. Marshall, A. Ghosh, I. Doss, Y. Ma, D. Stedman, B. Stinson, A. Varghese, M. Mohr, P. Rozario and S. Bhattacharyya, High-performance computing in undergraduate education at primarily undergraduate institutions in Wisconsin: Progress, challenges, and opportunities, *Educ. Inf. Technol.*, 2024, **29**, 18451–18475.

11 W. Humphrey, A. Dalke and K. Schulten, VMD: visual molecular dynamics, *J. Mol. Graph.*, 1996, **14**, 33–38.

12 J. C. Phillips, R. Braun, W. Wang, J. Gumbart, E. Tajkhorshid, E. Villa, C. Chipot, R. D. Skeel, L. Kalé and K. Schulten, Scalable molecular dynamics with NAMD, *J. Comput. Chem.*, 2005, **26**, 1781–1802.

13 J. C. Phillips, D. J. Hardy, J. D. C. Maia, J. E. Stone, J. V. Ribeiro, R. C. Bernardi, R. Buch, G. Fiorin, J. Hénin, W. Jiang, R. McGreevy, M. C. R. Melo, B. K. Radak, R. D. Skeel, A. Singharoy, Y. Wang, B. Roux, A. Aksimentiev, Z. Luthey-Schulten, L. V. Kalé, K. Schulten, C. Chipot and E. Tajkhorshid, Scalable molecular dynamics on CPU and GPU architectures with NAMD, *J. Chem. Phys.*, 2020, **153**, 0441301–33.

14 N. Ostrowska, M. Feig and J. Trylska, Varying molecular interactions explain aspects of crowder-dependent enzyme function of a viral protease, *PLoS Comput. Biol.*, 2023, **19**, 1011054.

15 B. R. Brooks, R. E. Bruccoleri, B. D. Olafson, D. J. States, S. J. Swaminathan and M. Karplus, CHARMM: A program for macromolecular energy, minimization, and dynamics calculations, *J. Comput. Chem.*, 1983, **4**, 187–217.

16 B. R. Brooks, C. L. Brooks, A. D. Mackerell, L. Nilsson, R. J. Petrella, B. Roux, Y. Won, G. Archontis, C. Bartels, S. Boresch, A. Caflisch, L. Caves, Q. Cui, A. R. Dinner, M. Feig, S. Fischer, J. Gao, M. Hodoscek, W. Im, K. Kuczera, T. Lazaridis, J. Ma, V. Ovchinnikov, E. Paci, R. W. Pastor, C. B. Post, J. Z. Pu, M. Schaefer, B. Tidor, R. M. Venable, H. L. Woodcock, X. Wu, W. Yang, D. M. York and M. Karplus, CHARMM: The biomolecular simulation program, *J. Comput. Chem.*, 2009, **30**, 1545–1614.

17 J. Huang and A. D. Mackerell, CHARMM36 all-atom additive protein force field: Validation based on comparison to NMR data, *J. Comput. Chem.*, 2013, **34**, 2135–2145.